# On the link between pole-zero distance and maximum reachable damping in MIMO systems

Dimitri Piron [a,b,*], Shashank Pathak [a], Arnaud Deraemaeker [c], Christophe Collette [a,b]

[a] BEAMS Department, Université Libre de Bruxelles, Brussels, Belgium
[b] Department of Aerospace and Mechanical Engineering, Université de Liège, Liège, Belgium
[c] BATir Department, Université Libre de Bruxelles, Brussels, Belgium

ARTICLE INFO

ABSTRACT

This paper studies the possibility of extending the already proved link between the pole-zero distance and the maximum reachable damping ratio in single input single output (SISO) systems to multiple inputs multiple outputs (MIMO) ones. This extension is shown to be possible when the considered system presents specific properties: (i) it is equipped with collocated transducers with small authority, (ii) the system has a small modal density in the frequency band of interest and (iii) a low authority control law is used. It is indeed demonstrated that when these three conditions are satisfied, the analytical development of the closed-loop poles convergence is equivalent to the one observed with SISO cases, except that the anti-resonances are replaced by the transmission zeros (TZs). Consequently, it is concluded that the maximum reachable damping ratio is directly proportional to the pole-transmission zero distance for such MIMO systems. This conclusion is demonstrated with two numerical examples (a cantilever beam and a simply supported plate) and experimentally validated on a cantilever beam where all the studied systems are equipped with two collocated pairs of piezoelectric patches.

## 1. Introduction

The poles (natural frequencies) are of high importance when studying the dynamics of any flexible system. For example, the poles inform at which frequencies a bounded disturbance can lead to a very large system response due to the resonance phenomenon. Such a resonance effect can cause structural damages to the system or, in worst cases, the complete destruction of the structure. Control systems are therefore required to prevent such unwanted phenomenon by decreasing the level of the spurious vibrations. Different alleviation strategies have been developed during the last few decades such as passive damping (e.g. [1]), active damping (e.g. [2]) or hybrid damping (e.g. [3]). Physically, those damping strategies aim at reducing the resonance peaks by dissipating the vibration energy, which then leads to an acceptable level of the system response when it is subjected to some internal and/or external disturbances.

Although the information contained within the open-loop system poles are of high importance in the development of those three damping approaches, the TZs play a major role as well. Indeed, those TZs that are defined as the frequencies at which a non-zero actuation leads to a zero output response can have a strong impact on the achievable performance of the control strategy. For example, they provide a phase lead that compensates the phase lag brought by the poles which, in case of collocated systems, ensures that the open-loop phase lag can never drop below 180 degrees thanks to the interlacing property [4]. Moreover, and for SISO linear and time-invariant collocated systems with well separated modes, the maximum achievable damping directly depends

* Corresponding author at: BEAMS Department, Université Libre de Bruxelles, Brussels, Belgium.
  E-mail address: dimitri.piron@ulb.be (D. Piron).

on the distance between the poles and the zeros [5]. A quick analysis of the TZs of those collocated SISO systems allows therefore to obtain, for a reasonable computational cost, valuable information on the possible performance once in closed-loop. A study has recently been published in which the pole-zero distance is used to build a novel sensor–actuator placement criterion for collocated SISO systems, allowing to obtain a control architecture with high modal damping while using small computational resources [6]. Unfortunately, the link between pole-zero distance and damping has never been studied for MIMO systems. This paper aims therefore to extend this link from SISO to MIMO, allowing to obtain knowledge on the performance of the considered system at small cost, which can be highly valuable for a preliminary evaluation.

The second section recalls some properties of the TZs and the convergence of the closed-loop poles in MIMO systems. The third part analytically explores how the distance between the pole and the TZ for a specific mode is related to the maximum reachable damping ratio once in closed-loop. The fourth section illustrates this new link with two numerical examples (a cantilever beam and a simply supported plate) while the fifth one provides an experimental validation on a cantilever beam. Finally, some concluding remarks are given in the last section.

## 2. Properties of the transmission zeros in MIMO systems

In SISO systems, the TZs are the frequencies at which a non-zero signal injected in the actuator leads to a zero output response in the sensor, which is the reason why they are often called anti-resonance frequencies. When dealing with a MIMO system, the TZs are the frequencies for which there is no transmission from the inputs to all the outputs of the system. The TZs are therefore not simply equal to the anti-resonance frequencies of each individual entry of the transfer function matrix, they are associated to the global system.

The TZs of MIMO systems can be obtained by applying different approaches. One of the main techniques is based on the state space representation from which the system matrix is built [7,8]. Let us consider a MIMO system with $n$ degrees of freedom and $r$ collocated inputs–outputs pairs, which can be represented by its state space form as follows:

$$\dot{x}(t) = Ax(t) + Bu(t)$$
$$y(t) = Cx(t) + Du(t) \tag{1}$$

where $x(t) \in \mathbb{R}^{2n}$ is the state variable vector, $A \in \mathbb{R}^{2n \times 2n}$ is the state matrix, $B \in \mathbb{R}^{2n \times r}$ is the input matrix, $y(t) \in \mathbb{R}^r$ is the output vector, $C \in \mathbb{R}^{r \times 2n}$ is the output matrix and $D \in \mathbb{R}^{r \times r}$ is the feedthrough matrix. Eq. (1) can be easily rewritten in the Laplace domain and rearranged as follows:

$$\begin{bmatrix} sI - A & -B \\ C & D \end{bmatrix} \begin{bmatrix} x \\ u \end{bmatrix} = \begin{bmatrix} 0 \\ y \end{bmatrix} \tag{2}$$

where $s$ is the complex Laplace variable and the left hand side matrix is called the system matrix. Since the TZs are the frequencies at which all the outputs of the system are zero when applying non-zero inputs, they are the solution of Eq. (2) when $y$ is set to zero:

$$\begin{bmatrix} Z_0 I - A & -B \\ C & D \end{bmatrix} \begin{bmatrix} x_0 \\ u_0 \end{bmatrix} = \begin{bmatrix} 0 \\ 0 \end{bmatrix} \tag{3}$$

Hence, the solutions of Eq. (3), which are obtained by solving the generalised eigenvalue problem, provide the different TZ frequencies $Z_0$. Interestingly, each TZ is related to a specific zero input direction $u_0$ while, in case of SISO systems, a particular input signal is not required. This is due to the switching from scalar space (i.e. with SISO systems) to the vectorial one (in case of MIMO systems), in which the input vector cannot be cancelled out before solving the equation.

The TZs can also be computed from the transfer function matrix representation, which can be obtained by transforming the state space system of Eq. (1) as follow [9]:

$$G(s) = C(sI - A)^{-1} B + D \tag{4}$$

where $G(s) \in \mathbb{R}^{r \times r}$ is the transfer function matrix and $I \in \mathbb{R}^{2n \times 2n}$ is the identity matrix. Usually, the TZs of the system cannot be computed with the transfer matrix in its original coupled form. Therefore, a Smith–McMillan reduction is performed [10,11], which allows to obtain a diagonal canonical form of the system. Nevertheless, applying the Smith–McMillan reduction instead of using the state space representation to compute the TZs can lead to some complications, such as (i) additional effort required to obtain the zero input directions $u_0$, (ii) numerical imprecisions when solving the Smith–McMillan reduced form or (iii) the omission of the TZ frequencies related to the uncontrollable and/or unobservable subsystems [12].

Finally, the TZs of MIMO systems with collocated displacement sensor-force actuator pairs correspond to the eigenvalues of an associated constrained problem [13]. Hence, the TZs of such configurations can be obtained by solving the corresponding eigenvalue problem, which is already well-known and used in SISO systems [14]. Nonetheless, this physical interpretation does not hold for non-collocated configurations where the TZs are obtained by solving a non-symmetric eigenvalue problem which leads to non-minimum phase zeros [15].

It is also well known that, in SISO system, the closed-loop poles tend to the open-loop anti-resonances for high value of the feedback gain. Nevertheless, and as previously discussed, MIMO systems present (1) the anti-resonance frequencies that are related to each sensor–actuator combination and (2) the TZs that are associated to the global system. The question of the convergence of the closed-loop poles in such MIMO systems is therefore important.
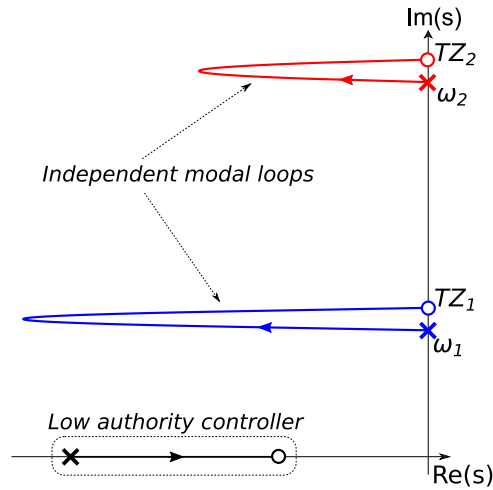
**Fig. 1.** Hypothesis on the shape of the root locus in case of a MIMO decentralised low authority controller with small modal density and a TZ in the vicinity of each open-loop pole.

It has first been proved by Davison [16] and then analytically confirmed by Preumont [17] that when dealing with collocated MIMO systems, the closed-loop poles that do not tend to infinity when increasing asymptotically the gain are converging towards the TZs. Moreover, this asymptotic behaviour does not depend on the feedback control law, unlike the shape of the root locus. Besides, it is stated in [17] that it is not possible to predict the precise trajectory of the closed-loop poles in the complex plane.

Nevertheless, and despite this last statement, it can be actually shown that in case of a low authority controller with a specific architecture, the shape of the root locus can present an expected trajectory, as demonstrated in the next Section.

## 3. Pole-TZ distance and maximum reachable damping in MIMO

The impossibility of predicting the shape of the root locus for MIMO systems depicted in [17] is mainly due to its generalisation for any type of controller. Indeed, specific configurations can lead to expected behaviours similar to SISO systems and, therefore, the possibility to draw the root locus of the closed-loop system using only the open-loop poles and the TZs knowledge.

Let us consider a flexible system with almost no damping and a small modal density on which multiple collocated sensor–actuator pairs are mounted. For some transducer configurations, it can be assumed that a TZ lies in the vicinity of each open-loop pole, mimicking therefore the alternating pole-zero property of the SISO collocated systems. By recalling the physical interpretation of the TZs (i.e. they correspond to the frequencies of an associated constrained system), this condition is only possible when the transducers present a small authority on the system such that the corresponding constrained system is close to the unconstrained one. This can for example be observed when only a few force actuator-displacement sensor pairs are mounted on a very large system. When considering piezoelectric patch actuation, small authority occurs when the cumulated size of the patches is small with respect to the size of the system or when the patches are located in an area with small amount of strain energy.

When a control law is implemented, the closed-loop poles of the controlled system converge towards the TZs for large gain values. If the implemented controller presents a small authority, its effect is limited which restricts the migration of the closed-loop poles in the complex plane. Moreover, and because of the small modal density hypothesis, the different open-loop poles are located far away from each other, limiting therefore the possible modal interaction. Consequently, each open-loop pole converges towards the TZ in its neighbourhood, forming thereby independent modal loops. This hypothesis is illustrated in Fig. 1 where the real and the imaginary axes present different scale in order to ease the visualisation.

Independent root loci derived from each open-loop pole and the TZ in its neighbourhood can therefore be considered, allowing to analyse the migration of every closed-loop pole independently by only considering the open-loop pole, the TZ in its neighbourhood and the low authority control (LAC) law. Let us for example consider a decentralised architecture with an identical LAC law, such as an integral force feedback defined by:

$$C(s) = g \, \frac{1}{s} \tag{5}$$

where $g$ is the gain of the controller. Because of the independent behaviour of each mode, the characteristic equation of the closed-loop system can be written in the modal coordinates as follows:

$$1 + g \, \frac{1}{s} \left( \frac{s^2 + Z_{0,i}^2}{s^2 + \omega_i^2} \right) = 0 \tag{6}$$

where $\omega_i$ is the open-loop pole of the mode of interest $i$ and $Z_{0,i}$ is its related TZ, i.e. the TZ that lies in the vicinity of $\omega_i$ in accordance with the hypothesis. The full path of each closed-loop pole in the complex plane can thereby be computed by solving Eq. (6) when the gain $g$ is varied from 0 to infinity.

Interestingly, Eq. (6) presents the same form as the characteristic equation of a SISO integral force feedback controller architecture from [5], the only difference being that the anti-resonance $z_i$ in the SISO configuration is replaced by the TZ values $Z_{0,i}$ in the considered MIMO architecture. Therefore, the existing link between the maximum reachable damping of mode $i$, $\xi_i^{max}$, and the pole-zero distance in collocated SISO systems that has been demonstrated in [18] can be extended to collocated MIMO ones by replacing the anti-resonance frequency $z_i$ with the TZ value $Z_{0,i}$, which leads to:

$$\xi_i^{max} = \frac{Z_{0,i} - \omega_i}{2\omega_i} \tag{7}$$

Consequently, Eq. (7) shows that the link between damping and pole-zero distance holds in the case of MIMO systems. Nevertheless, this relationship is only valid when the three hypotheses that have been previously defined are satisfied, i.e. when (1) the considered system presents a small modal density, (2) a TZ lies in the vicinity of each open-loop pole and (3) the collocated control architecture has a small authority. Those properties can be encountered in different engineering applications such as communication antennas, solar panels or large mirrors for observatory purposes. Indeed, it is for example illustrated in [19] that a laminated membrane plate mirror modelled for space telescopes presents a small modal density for the first four modes. Hence, and as it will be demonstrated in the numerical and experimental validation sections, mounting collocated pairs of piezoelectric patches on such system induces TZs in the vicinity of the poles, guaranteeing therefore the hypotheses.

Obviously, the expression of the maximum reachable modal damping given by Eq. (7) is only valid when a integral force feedback controller is applied. However, and even though using another control law can modify this expression, the maximum achievable damping will still be directly proportional to the distance between the open-loop pole $\omega_i$ and the nearby transmission zero $Z_{0,i}$. It is indeed shown in [5] that, for different SISO cases, the maximum damping ratio is always proportional to the pole-zero distance no matter which LAC is used. Hence, when the defined hypotheses are satisfied, and therefore when the modal loops are independent which allows to replace the anti-resonances by the TZs, a more general expression can be defined as follows:

$$\xi_i^{max} \propto |P\, Z_0|_i \tag{8}$$

where $|P\, Z_0|_i$ expresses the pole-TZ distance of mode $i$. This distance can be obtained by the difference between the TZ and the nearby open-loop pole when the system exhibits a pole-TZ pattern (as applied in Eq. (7)) or by the difference between the open-loop pole and the nearby TZ when the latter appears first.

The extension of the direct link between the maximum reachable damping and the pole-TZ distance for MIMO systems described by Eq. (8) is numerically demonstrated in the next section on two different systems: a cantilever beam and a simply supported plate. An experimental validation is also performed on a cantilever beam, proving therefore that the required three specific properties can be encountered on real-live structures.

## 4. Numerical validation

The extension of the direct link between the maximum reachable damping and the pole-TZ distance for MIMO systems described by Eq. (8) is subjected to some limiting hypotheses. The aim of this section is to provide numerical examples of systems that satisfy those required hypotheses in order to prove that, in such a case, this direct link exists. The numerical simulations have been performed using the Structural Dynamics Toolbox (SDT), an open and extendible finite element modelling MATLAB based toolbox for dynamics problems [20].

Two different systems have been considered: one with less modal density (a cantilever beam) and the other with a higher one (a simply supported plate). In both cases, the values of the TZs have been modified by changing the positions of the collocated transducer pairs. Moreover, the two systems are defined with the same lightly damped steel with the following properties: Young's modulus $E = 210$ GPa, Poisson's ratio $\nu = 0.285$, mass density $\rho = 7800\ kg/m^3$ and modal damping ratio $\xi = 0.004$.

The cantilever beam is modelled with the dimension of 300 mm $x$ 25 mm $x$ 2 mm and its finite element model is built with 6 degrees of freedom (DOFs) shell elements each 1 and 5mm in the $x$ and $y$ direction respectively, leading to 1806 nodes in total. Two lead zirconate titanate (PZT) piezoelectric voltage actuators and two PZT sensors patches are considered, with the following dimension: 15 mm $x$ 25 mm $x$ 0.5 mm. A possible position is defined every 30mm in the longitudinal direction of the beam starting from its clamped end, leading to 10 different placement locations. In order to perform this study on a MIMO system, two pairs of patches are placed together, translating consequently the 10 possible patch locations into 45 different configurations in total. Moreover, to ensure the collocation of the transducers in the sense that there is the alternating pole-zero property on the open-loop transfer function of each pair in the frequency band of interest, each sensor–actuator pair is placed at the same location but on the opposite sides of the structure for every tested configuration. Such configuration allows indeed to ensure this alternating properties within the frequency band of interest when dealing with piezoelectric patches, as demonstrated by [21]. The entire set of the 10 possible patch positions is shown in Fig. 2(a), as well as the Cartesian coordinates of the beam. Finally, and because the different considered pair positions do not allow to control the torsion modes (the patches are symmetrically placed along the middle transversal axis), the study will be limited to the bending modes of the beam.

The simply supported plate defined by free rotation but fixed translation on its four edges is modelled with the dimension of 300 mm $x$ 240 mm $x$ 2 mm and is discretised by 6 DOFs multilayer shell elements each 3mm in both $x$ and $y$ directions (8181 nodes
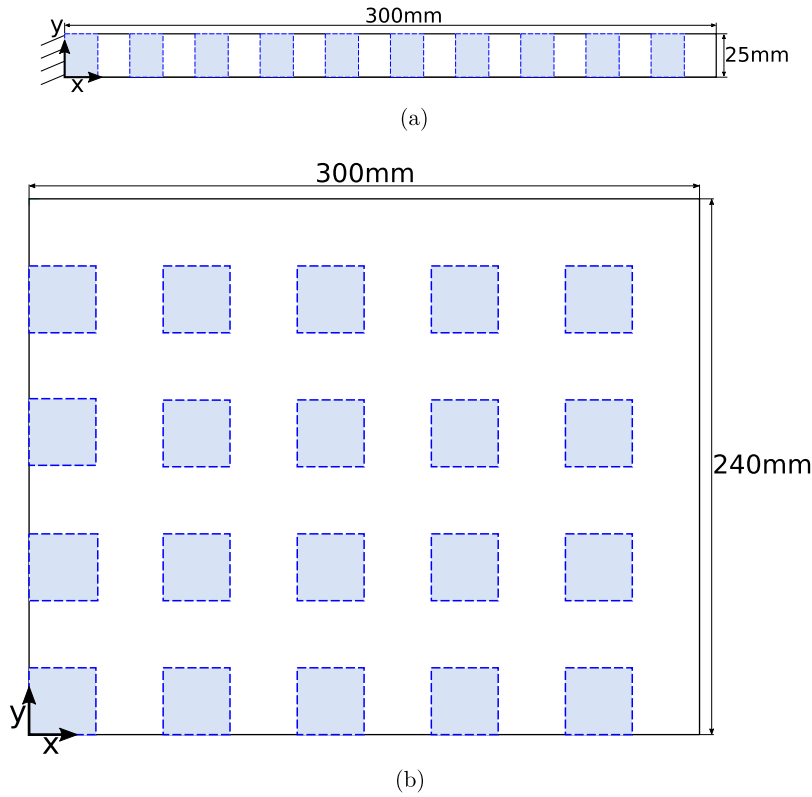
**Fig. 2.** Representation of the two structural systems and the full set of possible patch positions in dotted blue lines: (a) top view of the cantilever beam that presents 10 possible patch positions along its longitudinal axis *x*, (b) top view of the simply supported plate with a total of 20 possible patch positions in the *x* and *y* directions.

in total). Again, two pairs of PZT piezoelectric voltage actuators and sensors patches are considered, with the following dimension: 30 mm *x* 30 mm *x* 0.5 mm. A pair of patches can be placed each 60mm in both the *x* and *y* directions starting from the origin of the Cartesian frame, leading to 20 possible patch positions. Because two pairs of patches are again considered, those possible positions translate into a total of 190 different configurations. The alternating pole-zero property within the frequency band of interest is again ensured by placing the actuator and sensor patches at the same location but on opposite sides of the structure, for each considered configuration. The entire set of the 20 possible patch positions is shown in Fig. 2(b), as well as the Cartesian coordinates of the plate.

Regarding the control architecture, a decentralised identical direct velocity feedback (DVF) control law is selected. Such LAC introduces indeed only one parameter (the gain *g*), which avoids any additional variability in the control architecture when analysing the results obtained with the cantilever beam or the simply supported plate. Because the considered systems present, for each configuration, two collocated pairs of patches, the controller $C(s)$ is defined as a $2 \times 2$ matrix as follows:

$$C(s) = g \begin{bmatrix} s & 0 \\ 0 & s \end{bmatrix} \tag{9}$$

The root loci obtained for arbitrary configurations of the two systems when applying the decentralised controller defined by Eq. (9) are shown in Fig. 3. It can be seen that the three required conditions to ensure the MIMO extension are fulfilled. Indeed, (1) the open-loop poles of the considered modes are indeed well separated (low modal density), (2) a TZ lies within the vicinity of each open-loop pole (mimicking the alternating pole-zero property of collocated SISO systems) and (3) each mode behaves independently from the others by making a loop from the open-loop poles towards the surrounding TZ (low authority control with no modal interaction). This therefore confirms the possibility to encounter systems that present the aforementioned conditions and, consequently, it reassures about the relevance of the presented extension of the link between damping and pole-zero distance for MIMO systems expressed by Eq. (8).

It can be seen in Figs. 3(a) and 3(b) that, for each configuration and each mode, an optimal gain value allows to obtain the maximum reachable damping ratio, i.e. the one obtained at the leftmost position of the closed-loop poles in the complex plane. Hence, the maximum reachable damping ratio can be easily extracted for each of the first three modes, for the entire set of the 45 (cantilever beam) and 190 (simply supported plate) possible pairs configurations.

Moreover, the value of all the TZs can be obtained by using the state-space approach developed in the previous Section. Hence, and in addition to the maximum reachable damping ratio of each mode, the pole-TZ distance can be computed as well by calculating
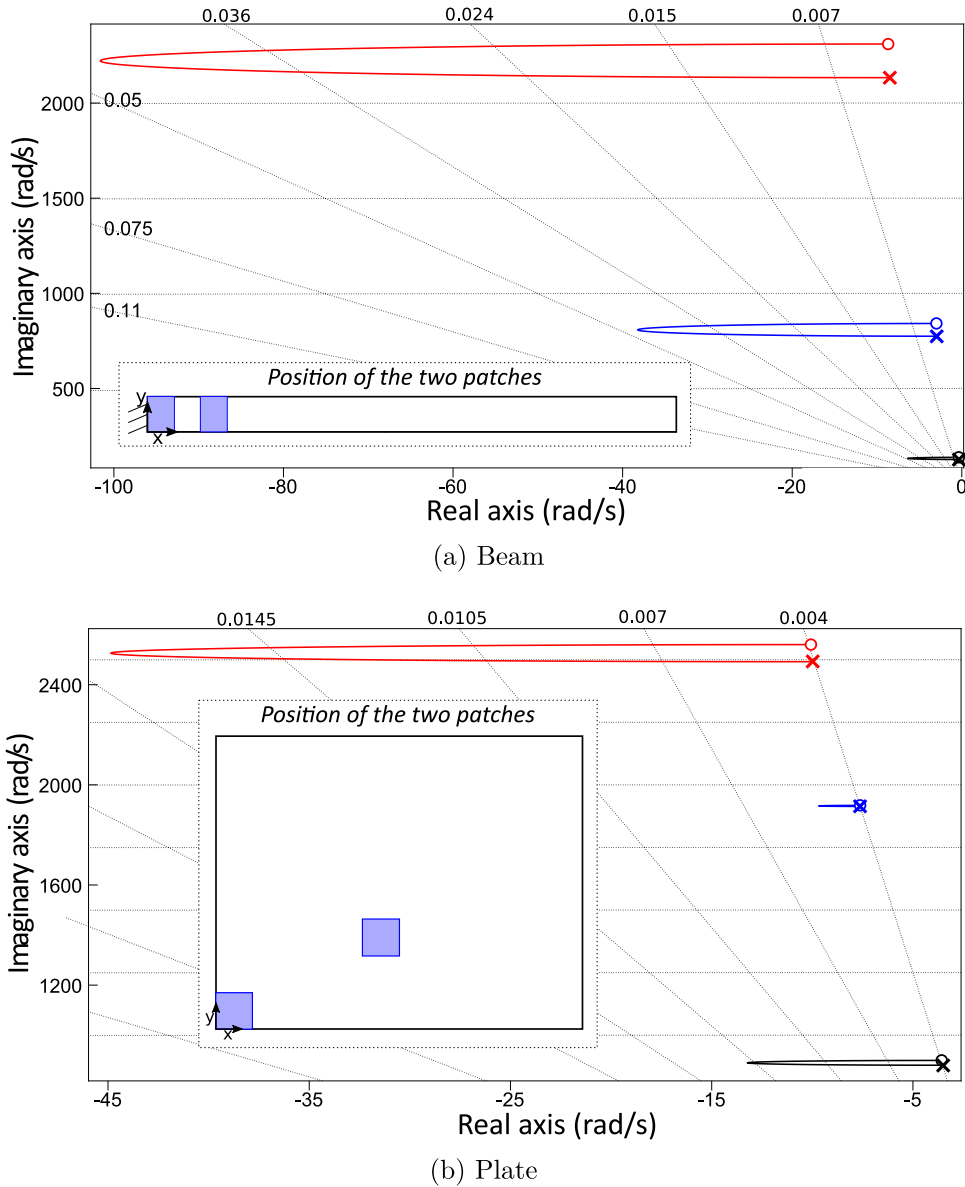
(a) Beam



(b) Plate

**Fig. 3.** Root locus in closed-loop with an identical decentralised DVF controller for specific locations of two pairs of piezoelectric patches on: (a) the cantilever beam, (b) the simply supported plate.

the difference between each TZ and each surrounding pole, for all the possible pair configurations. It therefore means that the link between the maximum reachable damping ratio and the pole-TZ distance can be plotted for all the considered configurations and for the first three modes of the two systems. In order to ease the visualisation of this link for those three modes, the pole-TZ distance needs to be normalised to ensure the same order of magnitude for each mode. Consequently, the normalised pole-TZ distance $|P\ Z_0|_{i,norm.}$ of mode $i$ is defined by:

$$|P\ Z_0|_{i,norm.} = \frac{Z_{0,i} - \omega_i}{\omega_i} \tag{10}$$

Figs. 4(a) and 4(b) show, for the cantilever beam and the simply supported plate respectively, the value of the maximum reachable damping ratio as a function of the corresponding normalised pole-TZ distance for the three first modes of interest. In addition, the dotted lines plotted on both figures correspond to a first-order fit based on a least-squares approach using the entire set of entries. The two figures clearly highlight the proportionality between the maximum reachable damping ratio and the pole-TZ distance, demonstrating therefore that the generalised linear link expressed by Eq. (8) is verified for the two considered systems and all the modes of interest. Furthermore, and for each system, this linear link exhibits a common factor for all the modes, meaning
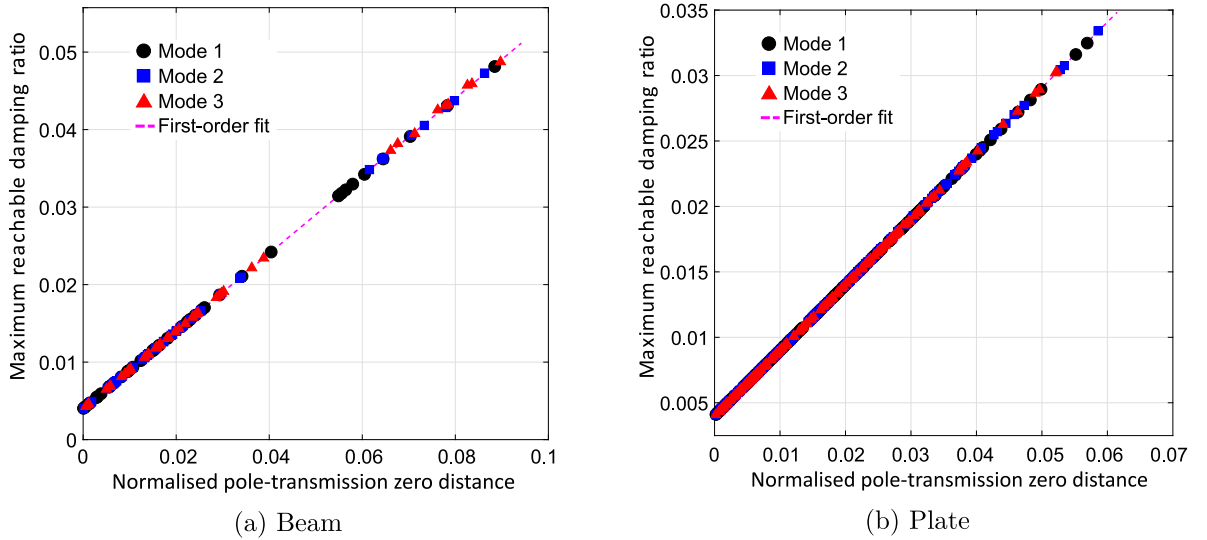
(a) Beam                                                    (b) Plate

**Fig. 4.** Maximum reachable damping ratio as a function of the normalised pole-TZ distance for the first three modes: (a) for the cantilever beam, (b) for the simply supported plate.

that it is indeed possible to find the analytical expression of the damping as a function of a normalised pole-TZ distance such as the one formulated by Eq. (7). Those observations are therefore numerically proving the presented extension of the link between damping and pole-zero distance for collocated SISO systems to MIMO ones when the different defined conditions are satisfied. The next section experimentally demonstrates this extension on a cantilever beam.

## 5. Experimental validation

In order to experimentally validate the presented extension, a model in SDT is first implemented to determine the appropriate parameters of the experimental system, the size and the position of the active patches and the method that will be applied to estimate the performance index. This analysis provided the following system: the structure consists in a 250 mm x 36.4 mm x 0.75 mm cantilever steel beam. The same steel used for the numerical validation is used again to build the model, the only difference being that the modal damping ratio has been set to $\xi = 0.01$ instead of 0.004 in order to comply with the damping introduced by the effect of non-perfect clamping. Five pairs of 13 mm x 13 mm identical piezoelectric patches are mounted with a spacing of 3 mm between them in the longitudinal direction and symmetrically to the central axis. The patches consist of $d_{31}$ P2 Macrof Fiber Composites (MFC) which have been ordered with a specific size and wiring scheme from Smart Material company (not in the regular catalogue), with an overall thickness of 0.3 mm (0.18 mm for the active layer) and a volume fraction of active fibres of 86% as for the normal MFCs from the catalogue. It can be noted that the MFC active layer is modelled with equivalent piezoelectric properties obtained with homogeneization, as explained in [22]. Similarly to the numerical validation, each sensor–actuator pair is placed at the same location but on the opposite sides of the structure. Moreover, another piezoelectric patch ($d_{33}$ PZT type) of dimension 34 mm x 7 mm (in the longitudinal and transversal directions, respectively) is attached at the root of the beam in order to excite the structure. The entire system is modelled with a total of 16800 shell elements. Finally, the Young modulus of the elements located near the vicinity of the clamp has been increased by 2% to model the non-perfect clamping, as illustrated in Fig. 5(a) by the use of a different colour for those elements; a picture of the experimental setup is shown in Fig. 5(b) as well.

As considered for the numerical validation, configurations composed by two pairs of sensors–actuators patches are investigated. Because 5 locations are available, a total of 10 different MIMO configurations can be studied; each one being composed by two pairs of active patches. To avoid the addition of an extra transducer, one of the three unused MFC sensor patches will be chosen to measure the response of the system. Consequently, the five pairs of patches that are mounted on the beam can be sorted as follow, for each configuration: two pairs are dedicated for the control loop, two are not in use (i.e. open circuit connexion) while the sensor of the last pair is used to measure the response of the system.

Similarly to the numerical validation, a decentralised identical control law is selected as the control architecture. Nevertheless, and to avoid spillover issues or excessive sensor noise amplification, a first order positive position feedback (PPF) is chosen instead of a DVF. Indeed, the PPF control law provides a −20 dB/decade roll-off which is compulsory for systems that present non-negligible dynamics at high frequency, such as the considered voltage/voltage pairs of piezoelectric patches [23]. Because this study will be limited to the first two bending modes, the filtration pole of the PPF is set to $\omega_c = 530$ rad/s, i.e. $\omega_c = 1.25 \times \omega_2$ where $\omega_2$ is the second natural pulsation of the beam. Hence, the controller $C(s)$ is defined as a $2 \times 2$ matrix as follows:
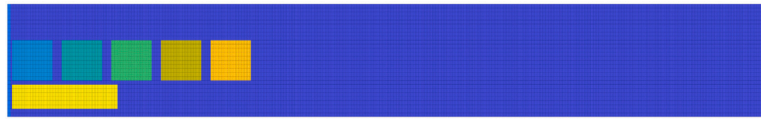
(a) Finite element model
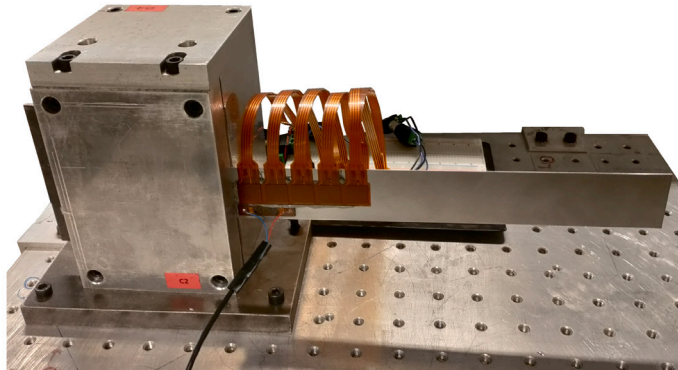


(b) Experimental setup

**Fig. 5.** Side views of the experimental system with the five MFC sensor patches and the disturbance PZT patch: (a) finite element model built within SDT, (b) the experimental setup.
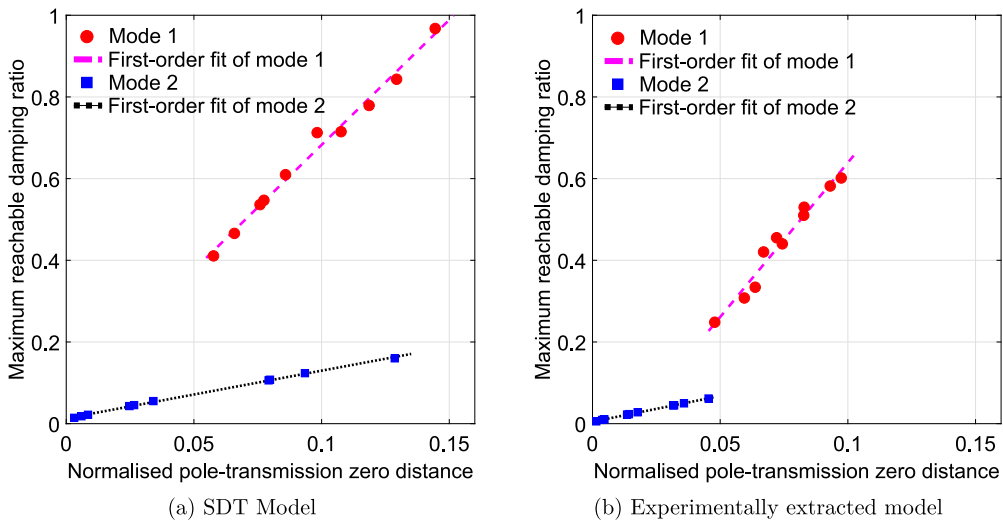


(a) SDT Model



(b) Experimentally extracted model

**Fig. 6.** Maximum reachable damping ratio as a function of the normalised pole-TZ distance for the first two modes: (a) from the SDT model, (b) from the experimentally extracted model.

$$C(s) = \frac{-g}{s + \omega_c} \begin{bmatrix} 1 & 0 \\ 0 & 1 \end{bmatrix} \tag{11}$$

Although the use of the finite element model is of high interest to design the experimental setup and to ensure its desired behaviour, it is well known that deviations will appear between the model and the experimental setup. Those deviations can be attributed to different factors, e.g. the inaccuracy of the material parameter values, imprecision on the placement of the patches during the mounting, the effect of the glue that is not considered in the model or the difficulty to accurately model piezoelectric structures because of the interaction between mechanical and electrical effects [24]. Consequently, an experimentally extracted model is built for all the ten configurations by first measuring the open-loop responses between the different patches and secondly by fitting those experimental transfer functions using the modal identification toolbox available within SDT. The identification method is based on the fitting of a pole-residue type model, with both high and low frequency corrections, which can then be transformed into a state-space representation. Using the finite element model and the experimentally extracted one, the link between the maximum
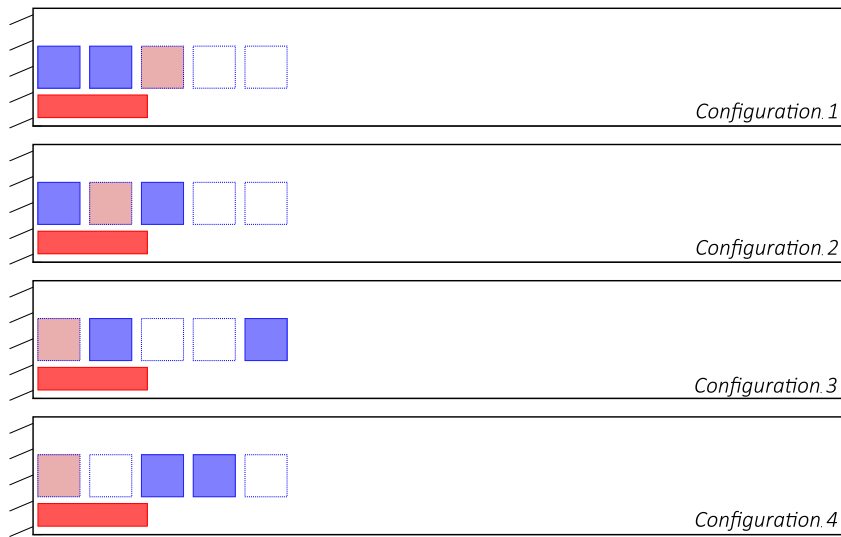
**Fig. 7.** Illustration (top view) of the four configurations that have been experimentally tested. For each configuration, the filled blue patches are the MFC active ones used in the control loop, the red patch corresponds to the PZT disturbance actuator and the pink patch is the MFC used as a sensor to build the performance index.

reachable damping and the normalised pole-TZ distance can be plotted for the 10 configurations and for the first two considered modes, as previously done in the numerical validation. As shown in Fig. 6, the direct link between the maximum damping and the pole-TZ distance is again numerically established for this new system on the two different models. Nevertheless, and for both the models, a modification of the slope factor can be observed between the two modes, which can be explained by the filtration pole $\omega_c$ and its variable interaction on them. Moreover, and although the same overall behaviour is observed, the SDT model presents higher maximum reachable damping ratio and higher normalised pole-TZ distance compared to the experimentally extracted model. This overestimation is due to the fact that the finite element model exhibits larger pole-TZ distances than the ones obtained with the experimentally extracted one, increasing consequently the damping. Additionally, the extracted model presents different damping values for each pole and anti-resonance which modifies the shape of the different root loci [25], impacting therefore the maximum reachable damping.

In order to experimentally validate the linear link obtained with the experimentally extracted model, a dSPACE MicroLabBox is used for both the data acquisition and the control aspect, with the sampling frequency set to 20 kHz. Moreover, and because the capacitance of the MFC patches is low (approximatively $18nF$), a sensor signal conditioner from PCB Piezotronics (model 482C) with unitary gain is used to avoid any possible impedance issue in case of direct connection from the patches to the MicroLabBox.

The experimental test campaign focusses on four of the ten available configurations such that all the patches are in use at least once, as illustrated by Fig. 7 where the active patches for each selected configuration are filled in blue while the MFC sensor patches used for the performance index are highlighted in pink. Additionally, the configuration scheme of the experimental study is depicted in Fig. 8 for the first considered configuration: a white noise generator is employed to excite the structure from 0 Hz to 300 Hz through the disturbance patch and the induced response of the system is measured by one of the MFC sensor. Simultaneously, the control architecture is applied on the two pairs of active patches while the unused remaining ones are kept open.

The experimental validation is done by the comparison between the theoretical and the experimental root-locus for each of the four considered configurations. Indeed, if the trajectories of the closed-loop poles in the complex plane obtained with the experimental set-up match the numerical ones for the different tested configurations, it can be assumed that the correlation for the other six is also validated. Therefore, the maximum damping ratio obtained with the numerical simulation and the TZ values are confirmed and, consequently, the linear link between the maximum damping ratio and the pole-TZ distance shown in Fig. 11(b) is validated. To obtain the experimental closed-loop poles, four different values of the gain $g$ from Eq. (11) are tested on the four configurations. For each gain value, the transfer function from the disturbance to the MFC sensor patches is measured. Then, the poles are obtained by fitting the experimental closed-loop transfer function using again the modal identification toolbox available within SDT. The comparison between the theoretical and the experimental closed-loop poles convergence, for each considered configuration, is shown in Fig. 9 where the coloured solid lines correspond to the simulated root locus using the experimentally extracted model and the black crosses represent the closed-loop poles for the considered gain values. As it can be seen, none of the four selected gains ($g = 2500$, $g = 5000$, $g = 7500$ and $g = 10000$) is sufficient to reach the maximum damping value for none of the two modes and any of the four configurations. This is because the first order PPF is not unconditionally stable: the additional pole brought by the control law on the real axis converges indeed towards the right half plane for large gains, limiting consequently its value [5]. Nevertheless, the trajectory of the closed-loop poles in the complex plane is correctly mimicking the simulated closed-loop behaviour, validating therefore the simulated root loci and, consequently, the maximum reachable damping values as well as the
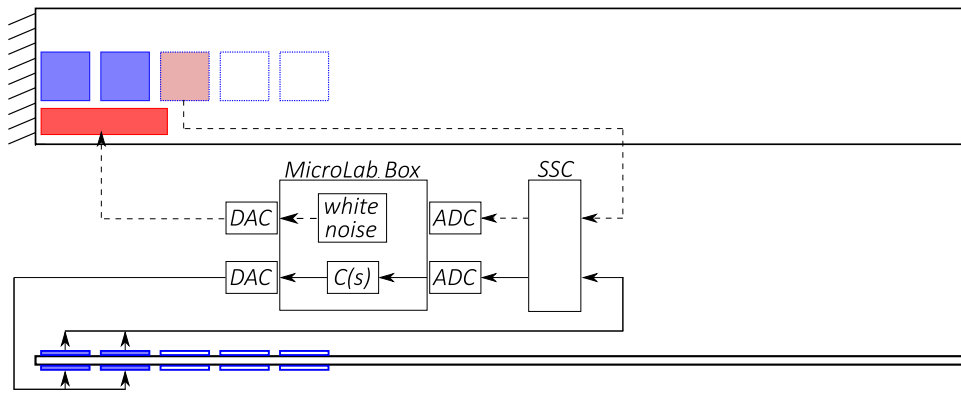
**Fig. 8.** Top and side views of the control scheme (solid lines) and the performance index loop (dashed lines) for the experimental study of the first considered configuration. (ADC: Analog-to-Digital-Converter; DAC: Digital-to-Analog-Converter; SSC: Sensor Signal Conditioner).

TZ positions. Indeed, the slight mismatches that can be observed are attributed to the unavoidable errors arising from the modal identification on the damped systems evaluated to obtain the poles as well as on the experimentally extracted model. It can be noted that although the maximum reachable damping ratio is not attainable before the destabilisation of the system (in this specific case or for any other ones), the knowledge of the pole-TZ distance is still highly valuable. Indeed, having a high value of the maximum reachable damping translates to a system that exhibits its closed-loop poles further into the left half plane and a good authority for the corresponding mode.

In addition to the analysis of the closed-loop poles convergence, the comparison between the loop gain functions (i.e. the multiplication of the open-loop system dynamics with the controller) can be performed. It is indeed possible to experimentally measure the loop gain function between each actuator/sensor pair by cutting the loop within the MicroLabBox (between the controller and the digital-to-analog converter, see Fig. 8) and by injecting directly white noise to the actuator while measuring the output of the controller. The benefit of such approach is that it allows to avoid stability concerns when applying high gain values and, consequently, it allows to study the dynamics of the experimental setup for such unreachable gains in closed loop condition. The comparison between the experimental loop gains and the numerically estimated ones for the five pairs of MFC patches and for $g = 12438$ are shown in Figs. 10 to 12 (this gain value provides the maximum reachable damping for second mode when considering the first configuration). As it can be seen, the loop gain functions obtained experimentally are perfectly following the numerically estimated ones. This therefore confirms again the proper correlation between the experimentally extracted model and the experimental setup results, which demonstrates the experimental validation of the linear link between the pole-TZ distance and the maximum reachable damping as shown in Fig. 11(b).

## 6. Conclusion

The direct link between the pole-zero distance and the maximum reachable damping ratio is well established in collocated active control when dealing with low authority SISO systems. In this study, the possibility to extend this well-known link from SISO systems to MIMO ones is investigated. It is shown that such an extension is possible when the considered system presents the three following conditions: (1) the transducers are collocated and present a small authority on the system which leads to the presence of a TZ in the vicinity of each pole of interest, (2) the considered system possesses a small modal density in the frequency bandwidth of interest, and (3) a LAC is used in the feedback loop. When those three conditions are satisfied, each open-loop pole within the bandwidth of interest converges towards its surrounding TZ once in closed-loop, forming therefore independent modal loops in the root locus. It is shown that in such a case, the analytical expression of the closed-loop pole convergence is similar to the one observed in specific SISO systems, the only difference being that the anti-resonances are replaced by the TZs. Consequently, the direct link between the maximum damping ratio and the pole-TZ distance is confirmed and the intended extension is validated. This conclusion has first been illustrated on two numerical systems: a cantilever beam and a simply supported plate, both equipped with two collocated pairs of piezoelectric patches. Moreover, the proposed extension has been experimentally validated on a cantilever beam, also equipped with two pairs of piezoelectric patches. It is shown that the numerical and the experimental systems present the three required properties and that the linear link between the maximum reachable damping ratio and the pole-TZ distance appears accordingly. This linear link between the pole-TZ distance and the damping in specific MIMO systems introduced in this study could provide valuable information on the possible performance once in closed-loop while requiring only open-loop knowledge. Requiring only the open-loop knowledge translates by reasonable computational cost, which can lead to a possible extension of this study: the use of this link to build a new sensor–actuator placement criterion for MIMO systems. Indeed, such placement criterion would allow to obtain the position of the transducers that maximises the maximum reachable damping once in closed-loop while requiring only open-loop calculations. Such extension could be the subject of further research.
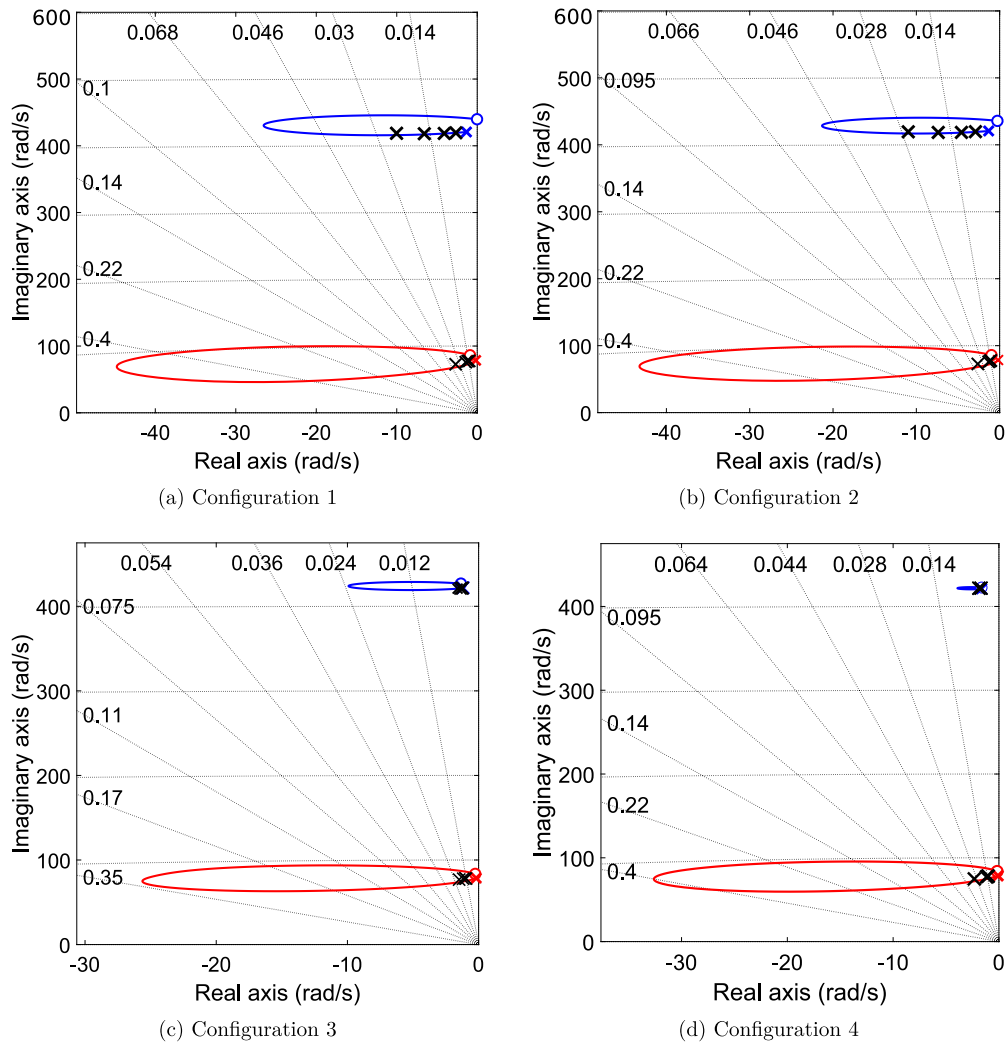
**Fig. 9.** Comparison between the simulated (coloured solid lines) and the experimental (black crosses) closed-loop poles convergence when applying the MIMO control architecture for the four considered configurations.
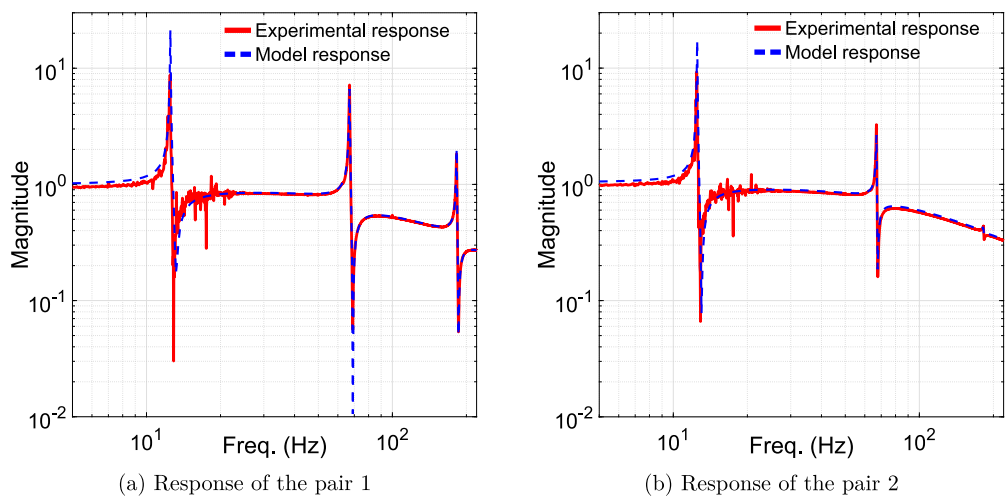


**Fig. 10.** Comparison between the experimental and the simulated loop gain functions with $g = 12438$: (a) on pair 1, (b) on pair 2.
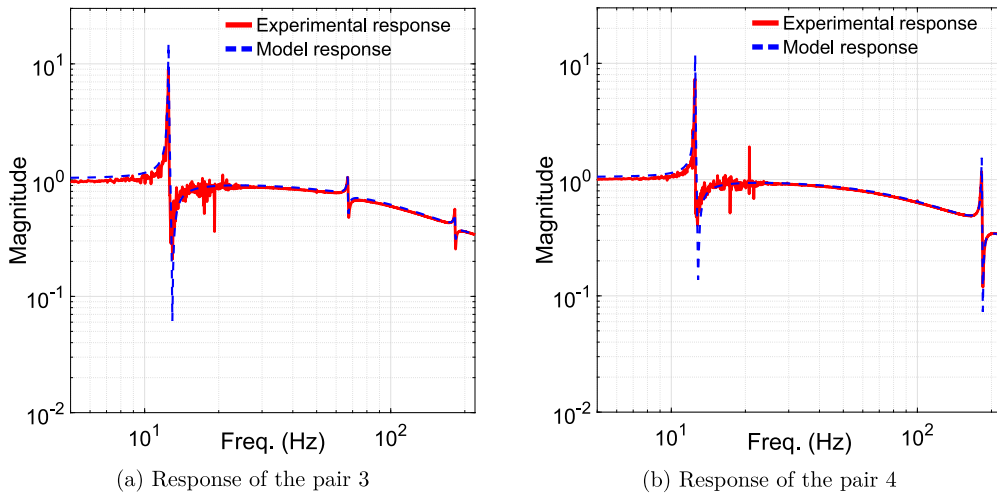
(a) Response of the pair 3          (b) Response of the pair 4

**Fig. 11.** Comparison between the experimental and the simulated loop gain functions with $g = 12438$: (a) on pair 3, (b) on pair 4.
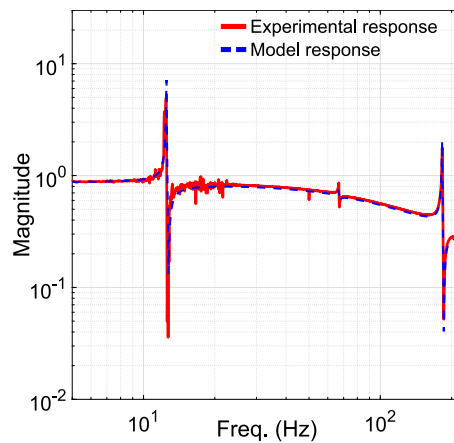


**Fig. 12.** Comparison between the experimental and the simulated loop gain functions with $g = 12438$ on pair 5.

## Declaration of competing interest

The authors declare that they have no known competing financial interests or personal relationships that could have appeared to influence the work reported in this paper.

## Acknowledgements

## References

[1] J.A.B. Gripp, D.A. Rade, Vibration and noise control using shunted piezoelectric transducers: A review, Mech. Syst. Signal Process. 112 (2018) 359–383.

[2] Guoying Zhao, Ghislain Raze, Ahmad Paknejad, Arnaud Deraemaeker, Gaëtan Kerschen, Christophe Collette, Active nonlinear inerter damper for vibration mitigation of duffing oscillators, J. Sound Vib. 473 (2020) 115236.

[3] Ahmad Paknejad, Guoying Zhao, Simon Chesné, Arnaud Deraemaeker, Christophe Collette, Hybrid electromagnetic shunt damper for vibration control, J. Vib. Acoust. 143 (2) (2021) 021010.

[4] Gary D. Martin, On the Control of Flexible Mechanical Systems (Ph.D. thesis), Stanford University, 1978.

[5] A. Preumont, Vibration Control of Active Structure, an Introduction, thrid ed., Springer, 2011.

[6] Dimitri Piron, Shashank Pathak, Arnaud Deraemaeker, Christophe Collette, A pole-zero based criterion for optimal placement of collocated sensor-actuator pair, Mech. Syst. Signal Process. 155 (2021) 107533.

[7] W.S. Levine, The Control Handbook in Two Volumes, CRC Press, 1999.

[8] W. Wolovich, On determining the zeros of state-space systems, IEEE Trans. Automat. Control 18 (5) (1973) 542–544.

[9] W.K. Gawronski, Advanced Structural Dynamics and Active Control of Structures, Springer-Verlag, New York, 2004.

[10] Thomas Kailath, Linear Systems, Prentice-Hall, 1980.
[11] J.M. Maciejowski, Multivariable Feedback Design, Addison-Wesley, 1989.
[12] A.G.J. Macfarlane, N. Karcanias, Poles and zeros of linear multivariable systems: a survey of the algebraic, geometric and complex-variable theory, Internat. J. Control 24 (1) (1976) 33–74.
[13] T. Williams, Constrained modes in control theory: Transmission zeros of uniform beams, J. Sound Vib. 156 (1) (1992) 170–177.
[14] D.K. Miu, Physical interpretation of transfer function zeros for simple control systems with mechanical flexibilities, J. Dyn. Syst. Meas. Control 113 (3) (1991) 419–424.
[15] Trevor Williams, Transmission zeros of non-collocated flexible structures-finite-dimensional effects, in: Dynamics Specialists Conference, 1992, p. 2116.
[16] E.J. Davison, S.H. Wang, Properties and calculation of transmission zeros of linear multivariable systems, Automatica 10 (6) (1974) 643–658.
[17] André Preumont, Bruno De Marneffe, Steen Krenk, Transmission zeros in structural control with collocated multi-input/multi-output pairs, J. Guid. Control Dyn. 31 (2) (2008) 428–432.
[18] Andre Preumont, Matteo Voltan, Andrea Sangiovanni, Bilal Mokrani, David Alaluf, Active tendon control of suspension bridges, Smart Struct. Syst. 18 (1) (2016) 31–52.
[19] Yifan Lu, Marco Amabili, Jian Wang, Fei Yang, Honghao Yue, Ye Xu, Hornsen Tzou, Active vibration control of a polyvinylidene fluoride laminated membrane plate mirror, J. Vib. Control 25 (19–20) (2019) 2611–2626.
[20] Etienne Balmes, Structural dynamics toolbox 7.1 (for use with MATLAB), 1991.
[21] Shashank Pathak, Dimitri Piron, Ahmad Paknejad, Christophe Collette, Arnaud Deraemaeker, On transmission–zeros of piezoelectric structures, J. Intell. Mater. Syst. Struct. (2021).
[22] Arnaud Deraemaeker, Gilles Tondreau, Frédéric Bourgeois, Equivalent loads for two-dimensional distributed anisotropic piezoelectric transducers with arbitrary shapes attached to thin plate structures, J. Acoust. Soc. Am. 129 (2) (2011) 681–690.
[23] J.L. Fanson, T.K. Caughey, Positive position feedback control for large space structures, AIAA J. 28 (4) (1990) 717–724.
[24] S.O. Reza Moheimani, Andrew J. Fleming, Piezoelectric Transducers for Vibration Control and Damping, Vol. 1, Springer, 2006.
[25] Yazdan Bavafa-Toosi, Introduction to Linear Control Systems, Academic Press, 2017.